Chemical Engineering Journal 526 (2025) 170737

Contents lists available at ScienceDirect

Chemical Engineering Journal

journal homepage: www.elsevier.com/locate/cej

Impact of third-body colliders on ammonia pyrolysis and oxidation: Detailed kinetic modeling and mechanistic insights

Alessandro Stagni *, Timoteo Dinelli

Department of Chemistry, Materials, and Chemical Engineering "G. Natta", Politecnico di Milano, Milano, 20133, Italy

ARTICLE INFO

Keywords:
Ammonia
Hydrogen
Chemical kinetics
Collision efficiencies
Pressure dependency

ABSTRACT

A major challenge in the chemical kinetics of ammonia is the quantification of the role of the bath gas in pressure-dependent reactions, in the full operating space. To this purpose, this work systematically investigates the impact of third-body colliders on ammonia and ammonia/hydrogen pyrolysis and oxidation chemistry, through an integrated workflow: after incorporating recent high-level theoretical calculations into a comprehensive detailed kinetic model, the key pressure-dependent reaction rates were parametrized through a fitting procedure, obtaining average errors below 3% compared to the starting theoretical values, while explicitly accounting for collider-specific behavior. Validation against experimental data highlighted the impact of major colliders on ignition delay times, species profiles, and laminar flame propagation. It was found that recombination reactions involving NH_3, HNO, and HO_2 are significantly affected by the bath gas composition, including ammonia itself as a collider, which is often ignored in most kinetic models. Species profiles in both pyrolysis and oxidation conditions showed significant sensitivity to the collider-specific effects: specifically, ammonia third-body effect in the recombination reaction $H + O_2(+M) \rightarrow HO_2(+M)$ was found to play a major role in the inhibition of H_2 oxidation, confirming the previous hypotheses. On the other hand, laminar flame speeds exhibited a lower sensitivity, with deviations typically within experimental uncertainties. Finally, the impact of mixture rules in the kinetic predictions was assessed by considering the four pressure-dependent reactions for which theoretical data on ammonia-related collision efficiencies are currently available. It was found that adopting a more accurate reduced-pressure mixture rule instead of a linear mixing, important deviations in the pressure-dependent rate constants at higher pressures were observed, yet with a moderate effect on macroscopic observables like ignition delay time and laminar flame speeds.

1. Introduction

In the last decade, ammonia (NH_3) has gained increasing attention in the energy transition scenario as an energy carrier, thanks to its favorable physical properties and carbon-free nature [1]. However, its wide-range utilization as a fuel still faces important scientific and technological challenges, to be overcome before its full-scale implementation [2]. Among them, the major issues arise from the intrinsically weak combustion features of ammonia compared to fossil fuels: higher ignition delay times and heat of vaporization, extremely low laminar flame speeds, and narrow flammability limits. All of these make the retrofitting and adaptation of conventional combustion devices a challenging task [3]. Moreover, ammonia combustion is inherently associated with the significant formation of nitrogen oxides (NO_x) via the fuel-bound nitrogen path [4,5], which requires a thorough understanding of chemical kinetics to effectively mitigate emissions.

As a result, ammonia pyrolysis and oxidation chemistry have become an active research field in recent years [5,6]. Such area could greatly benefit from the decades of experimental and theoretical methods first developed for conventional fuels, which has triggered a rapid expansion of available experimental datasets, kinetic rate estimations, and consequently kinetic mechanisms: Alnasif et al. [7] recently identified 61 distinct ammonia kinetic mechanisms published over approximately the past 50 years up to 2023, a number so large that structured methodologies are often necessary to systematically quantify and compare their predictive performances [8,9]. In spite of these advances, few specific fundamental areas of ammonia chemistry are still poorly understood or are systematically neglected across the kinetic models. In 2018, Glarborg et al. [5] comprehensively reviewed the state of the art of NH_3 pyrolysis and oxidation, highlighting the key areas that still require fundamental research. Since then, significant advances have been made on many of these gaps, thus expanding the fundamental knowledge needed for detailed kinetic modeling.

However, one important aspect that has not yet received a systematic attention in ammonia kinetic mechanisms is the role of third-body

* Corresponding author.
E-mail address: alessandro.stagni@polimi.it (A. Stagni).

https://doi.org/10.1016/j.cej.2025.170737
Received 5 August 2025; Received in revised form 12 October 2025; Accepted 9 November 2025
Available online 13 November 2025

colliders in pressure-dependent reaction rates. The importance of collisional energy transfer is well recognized even for the combustion chemistry of conventional hydrocarbons, where it has often received limited attention [10,11]. Expectably, due to the hierarchy principle, this lack of knowledge impacts ammonia kinetics, too [12]. To accurately represent the pressure and temperature dependence of a given reaction rate in a fixed bath gas, the state-of-the-art methodology is the use of logarithmic interpolation schemes (PLOG keyword in the CHEMKIN standard) [10,13]. Such interpolation effectively maps reaction rates, regardless of the number of wells and channels involved in the underlying Potential Energy Surface (PES) [14,15]. However, the major drawback of such an approach is related to the fixed properties of the bath gas, according to the collider chosen for the theoretical study. This makes impossible, within the classical PLOG formalism, to capture mixture effects, i.e. where multiple bath gases are involved.

On the other hand, reviewing the available low-pressure rate constants evaluated in various bath gases [16] shows that H_2O, CO and CO_2 are typically several times more efficient colliders than N_2, whereas Ar and He, which are most often used as dilutants to perform fundamental experiments, are less efficient colliders [17].

Bertolino et al. [18] found that third-body efficiencies of diluents like H_2O and CO_2 dominate hydrogen ignition and speciation in MILD combustion conditions, and that a single third body efficiency parameter impacted model variance more than entire groups of sensitive reactions (up to 20%). They also showed that replacing TROE formulations with PLOG formats for fall-off reactions can cause errors up to 2000% in combustion targets when third-body efficiencies are not properly handled. Moreover, when NH_3 or NH_3-rich fuel blends are concerned, the potential role of ammonia itself as a collider adds further complexity. In recent years, this possibility has been highlighted both experimentally and theoretically: Sabia et al. [19] first performed an experimental campaign in a non-adiabatic Jet Stirred Reactor, and showed that several kinetic models were unable to predict the reactivity and speciation trends of H_2-NH_3-O_2 mixtures diluted in Ar or N_2, especially with increasing NH_3 addition. They hypothesized the key role of ammonia itself as a collider, enhancing the recombination reaction $H + O_2 (+M) \rightarrow HO_2 (+M)$. This conclusion was later restated by Manna et al. [20], who pointed out that, until then, this aspect had not been sufficiently considered in the literature.

At the theoretical level, Glarborg et al. [21] and Jasper [22] were the first to set up a workflow to systematically predict third-body collision efficiencies by combining automated *ab initio* PES construction with classical trajectories. They successfully validated the framework against the available experimental values, showing an average 25% deviation. A significant breakthrough of their work was the systematic evaluation of collision coefficients involving NH_3, providing theoretical confirmation of the hypothesis initially proposed by Sabia et al. [19]. Moreover, their results highlighted a strong temperature dependence of such coefficients, which were found to change by even a factor 2 from 300 K to 2000 K. This was later confirmed by the same research groups with regard to the HNO recombination reaction [23].

In spite of these advances, to the authors' knowledge, a comprehensive kinetic analysis of the impact of these findings on ammonia pyrolysis and oxidation chemistry has not yet been performed, due to some key limitations. First, while the low- and high-pressure limit rate constants might be feasibly estimated, the fall-off behavior is usually fully characterized only for a limited number of colliders [24], or even just one. Second, evaluating the overall mixture rate constant via the CHEMKIN-style superposition of collider-specific rates has recently been demonstrated as not always accurate [25–27]; instead, a reduced-pressure linear mixture rule has been shown to be more appropriate [28]. Recently, Singal et al. [29] demonstrated the application of a such rule to a subset of key reactions relevant to ammonia and hydrogen chemistry.

In this scenario, the aim of this study is quantifying the macroscopic impact of third-body collider effects on ammonia pyrolysis and oxidation chemistry. Building upon the literature review discussed above, key pressure-dependent reactions involved in ammonia combustion were first systematically identified. Species- and temperature-dependent collision efficiencies were then incorporated into an updated detailed kinetic framework. This methodology allowed to perform a wide-range investigation of the role of both rates and colliders in the different conditions of interest for ammonia combustion. Finally, the impact of adopting different mixture rules on the predictivity of the kinetic mechanism was discussed.

2. Materials and methods

This section outlines the workflow followed for this investigation. As a first step, a subset of key reactions was identified through a comprehensive review of the experimental datasets combined with sensitivity analysis (Section 2.1). Later, such rate constants were parametrized to include to role of the collider at variable temperature and pressure (Section 2.2). They were then integrated into an updated kinetic mechanism, described in Section 2.3.

2.1. Experimental database and reactions selection

Based on previous works [8,9,30], the experimental database was extended according to the latest available data on NH_3 and NH_3-H_2 pyrolysis and oxidation experiments. They cover a wide range of operating conditions in terms of temperature T, pressure P, equivalence ratio Φ and blending ratio X_{H_2} for NH_3-H_2 blends. The ignition delay times in shock tubes (ST) and rapid compression machine (RCM), speciation in jet-stirred reactor (JSR) and flow reactor (FR), and laminar flame speed (LFS) as obtained with a variety of methods (Constant-volume vessel, heat flux burner, imaging shock tube) were all considered. A full list of the included experiments is available in Table S2 of the Supplementary Material. They are also available on the SciExpeM platform [31,32] (available at https://sciexpem.polimi.it).

The key, pressure-dependent rate constants were identified by means of targeted sensitivity analysis on (i) NH_3, NO and N_2O mass fraction in ST, JSR and FR, (ii) OH mass fraction in ST and RCM, and (iii) mass flow rate in LFS-related experiments. Following the hierarchy principle, only the reactions involving NH_3 chemistry were considered. This preliminary step was performed by employing the most up-to-date mechanism from the research group [33].

2.2. Rate constants parametrization

The modeling of pressure-dependent reaction rates in gas-phase kinetic mechanisms has made significant progress in the latest decades. The most traditional approaches have relied on simplified formalisms such as the Lindemann model and its extensions (Troe, SRI), which were originally developed for single-well reactions [34,35]. Although these models include empirical parameters, they describe the basic physics of pressure-broadening through theoretically sound functional formulations. For elementary systems, this approach has a satisfactory performance with typical accuracies within 10%–20% [36]. However, when applied to complex multi-well, multi-channel reaction systems, additional phenomena such as channel switching and multiple transition states introduce complexities that result in lower accuracy [37]. Moreover, in these cases the Lindemann form and its extensions cannot capture even the qualitative behavior, as certain channels may exhibit non-monotonic pressure dependence [36]. These limitations motivate the development of more sophisticated approaches, such as mixture rules [28] or alternative parameterizations, to explicitly capture such complex pressure-dependent phenomena.

The state-of-the-art methodology for representing pressure and temperature dependence makes use of logarithmic interpolation schemes (PLOG keyword in the CHEMKIN standard). This approach is capable to accurately map reaction rates in wide pressure ranges, regardless

of the complexity of the underlying PES. However, a major limitation of the conventional PLOG model lies in its assumption of fixed bath gas properties, preventing to describe mixture effects where multiple colliders with different collision behaviors are present.

Although the Chebyshev parametrization is the most mathematically flexible approach, showing superior fitting capabilities for $k(T, P)$ relationships through the use of numerous parameters, to the authors' knowledge it has received limited adoption so far. This is mostly due to two main limitations: its lack of physical interpretability and its inability to extrapolate beyond prescribed limits, compromising the accuracy of simulations when applied outside the fitted parameter space.

The most recent theoretical advances have pointed out the importance of collisional energy transfer in pressure-dependent kinetics [21,22]. From a practical perspective, the collider-dependent behavior of rate constants introduces additional challenges for the related modeling. The collider-specific dependency of reaction rates requires computational frameworks capable of including more parametric dependencies at the same time. Beyond the accuracy needed for representing specific collider-dependent rate constants, the resulting impact of such parametrization choices on kinetic model predictions must be also quantified. This is critical for comparing the performance of different parametrization approaches and determining whether the increased complexity of collider-aware models justifies their implementation instead of simplified alternatives.

The most basic approach consists in defining independent separate reactions for each collider, characterized by their respective rate coefficients and combined via a linear superposition. However, as demonstrated by theoretical analysis, this approach can introduce significant errors in specific multi-component systems, particularly when strong colliders are present in high concentrations, due to neglecting nonlinear effects arising from different collisional energy transfer characteristics among bath gas species. While errors can be important in specific operating conditions, their magnitude depends strongly on the operating conditions and collider composition, which motivates the need for more advanced mixture rules [25,26,28,29,38].

The framework described below is aimed at accurately representing the overall behavior of multiple colliders in complex gas mixtures. The mixture rules provide a theoretically-grounded approach for weighting individual collider contributions according to their respective efficiencies and concentrations, thus enabling more accurate predictions of pressure-dependent kinetics in multi-component systems.

2.2.1. Multiple bath-gas modeling framework

Table 1 shows an overview of the methodologies available for computing the rate constant in the presence of multiple independent collider-specific reactions, each characterized by a different rate constant k_i. The theoretical foundations and implementation details are explained in the Supplementary Material. For consistency, we adopted the same terminology and abbreviations as Burke and co-workers [28,29], whenever applicable.

The Independent-Colliders approach is the simplest methodology for handling multiple-collider species. In this approach, the overall rate constant is evaluated by summing up the collider-specific contributions, without any weighting. This approach is based on the assumption that each collider gives its own contribution to the overall reaction rate, regardless of the gas mixture composition.

The Linear Mixing Rule with Pressure dependence (LMR-P) introduces a composition-dependent weighting by multiplying each collider-specific rate constant by its mole fraction. This approach recognizes that each collider's contribution should be proportional to its abundance in the gas phase. The LMR-P rule intrinsically accounts for the dependence of collisional processes on species concentrations: therefore, a highly efficient collider present in trace amounts may contribute less to the overall reaction rate than a moderately efficient collider present at high concentrations.

Table 1
Equations describing the different methodologies to account for an arbitrary number of independent colliders simultaneously. Note that compared to the original notation used by Singal et al. [29], the notation Λ (i.e., the absolute value of the least negative chemically significant eigenvalue of the master equation) is replaced with k for a more straightforward interpretation in the present context (see also [28]).

Name	Equations
Independent colliders	$k_{IC}(T, P, \mathbf{x}) = \sum_{i=1}^{\text{Ncoll}} k_i(T, P_i)$
LMR-P	$k_{\text{LMR-P}}(T, P, \mathbf{x}) = \sum_{i=1}^{\text{Ncoll}} k_i(T, P)\, x_i$
LMR-R	$k_{\text{LMR-R}}(T, P, \mathbf{x}) = \sum_{i=1}^{\text{Ncoll}} k_i(T, Pr)\tilde{X}_i$ $Pr_{\text{LMR-R}}(T, P, \mathbf{x}) = \frac{\sum_i k_{0,i}(T) x_i [M]}{k_\infty(T)}$ $\tilde{X}_i(T, P, \mathbf{x}) = \frac{k_{0,i}(T) x_i}{\sum_j k_{0,j}(T) x_j}$

Among the linear mixing rules, the Linear Mixing Rule with Reduced Pressure Weighting [25–29,38] (LMR-R) is the most advanced approach, being based on the observation that the rate constants of different colliders behave similarly at the same reduced pressure: thus, the reduced pressure, $Pr_{\text{LMR-R}}$, is calculated using a weighted average of the low-pressure rate constants for each collider. This creates a pressure scaling for the mixture that reflects the collective third-body efficiency of all the species. Normalized mole fractions ($\tilde{X}_i$), i.e. the fractional contribution of each species mapped to the reduced pressure, are computed based on the relative contributions of each collider to the overall collisional energy transfer rate according to their respective low-pressure rate constants ($k_{0,i}(T)$). This weighting scheme ensures that colliders with higher intrinsic third-body efficiencies (i.e. larger $k_{0,i}$ values) have a greater influence on the overall reaction rates, even when they are present in lower concentrations. The LMR-R method provides a theoretically-based treatment of third-body effects by explicitly accounting for the varying collision efficiencies of different species through their low-pressure rate constants, which proxy third-body effectiveness. This approach is advantageous for pressure-dependent reactions, as it captures the physics of collisional energy transfer, and accounts for the falloff behavior, strongly influenced by the nature of the third-body colliders. However, to date it has not been integrated into the CHEMKIN standard, while it is fully supported by Cantera, starting from version 3.1.0 [39].

2.2.2. Fitting methodology

In order to describe the collider-specific effects (including ammonia itself) and assess its impact on subsequent model predictions, the previously employed reactions available in PLOG format were converted into falloff-type formulations. Depending on the available data and reaction type, either a parametrization including a broadening factor (e.g. Troe) or a Lindemann one was adopted. In this way, collider-specific efficiencies can be accounted for through modified low-pressure limits rates. The conversion from PLOG to falloff was performed through a systematic optimization-based refitting procedure implemented using a differentiable framework built on JAX [60]. First, dense training data were generated from the original PLOG representations across the relevant operating space (typically $300\ \text{K} \leq \text{T} \leq 2500\ \text{K}$ and $0.001\ \text{atm} \leq \text{P} \leq 100\ \text{atm}$). For each reaction, initial estimates of the falloff parameters were obtained by fitting the high-pressure limit to the highest pressure PLOG data and estimating the low-pressure limit from the lowest pressure data divided by the total concentration. The TROE broadening parameters (α, T^{***}, T^{*}, T^{**}) were initialized using temperature-dependent heuristics based on the mean temperature of the evaluation range.

The refitting optimization used the L-BFGS algorithm [61] to minimize the root mean square logarithmic error (RMSLE) between the

Table 2
Selected reactions in the NH_3 oxidation mechanism. Reaction rate expression is modified Arrhenius $k = AT^{\beta}\exp\left(-\frac{E_{act}}{RT}\right)$. Units are cm, cal, mol, K.

ID	Reaction	A	β	E_{act}	Notes	Ref.
R1	$NH_2 + H (+M) \leftrightarrow NH_3 (+M)$	1.500×10^{14}	0.167	0.0	k_∞	[40]
		4.655×10^{30}	−4.103	3314.5	k_0 (N_2)	[41]
		1.556×10^{30}	−4.060	3524.6	k_0 (Ar)	[22], pw
		1.083×10^{29}	−3.655	2998.1	k_0 (O_2)	[22], pw
		3.182×10^{31}	−4.039	3859.0	k_0 (NH_3)	[22], pw
		2.363×10^{31}	−3.967	3920.6	k_0 (H_2O)	[22], pw
	Troe parameters: $\alpha = 0.492$, $T^{***} = 166.4$, $T^{*} = 1893$, $T^{**} = 6070$					pw
R2	$H + NO (+M) \leftrightarrow HNO (+M)$	1.500×10^{15}	−0.410	0.0	k_∞	[42]
		1.230×10^{21}	−1.912	−395.7	k_0 (N_2)	[41]
		3.869×10^{20}	−1.819	−435.0	k_0 (Ar)	[23], pw
		2.239×10^{21}	−1.973	36.4	k_0 (He)	[23], pw
		8.132×10^{21}	−1.978	−138.5	k_0 (NH_3)	[23], pw
		5.784×10^{21}	−1.821	−246.9	k_0 (H_2O)	[23], pw
		3.423×10^{22}	−2.278	20.4	k_0 (H_2)	[23], pw
	Troe parameters: $\alpha = 0.623$, $T^{***} = 6625$, $T^{*} = 186.7$, $T^{**} = 4659$					pw
R3	$OH + NO (+M) \leftrightarrow HONO (+M)$	1.100×10^{14}	−0.300	0.0	k_∞	[43]
		1.382×10^{27}	−3.656	1404.4	k_0 (He)	[44], pw
	Troe parameters: $\alpha = 0.780$, $T^{***} = 6310$, $T^{*} = 475.4$, $T^{**} = 4770$					pw
	Efficiencies: $N_2 = 2$, Ar = 1.1, $NH_3 = 6$					[45]
R4	$N_2H_2 (+M) \leftrightarrow NNH + H (+M)$	3.962×10^{28}	−4.392	70455.3	k_∞	[46], pw
		8.571×10^{39}	−6.762	70461.8	k_0 (N_2)	[46], pw
	Efficiencies: Ar = 0.7, $O_2 = 0.8$, $NH_3 = 6.0$, $H_2O = 5.7$					R5 [22]
R5	$NH_2 + NH_2 (+M) \leftrightarrow N_2H_4 (+M)$	5.600×10^{14}	−0.414	66.0	k_∞	[47]
		1.625×10^{34}	−5.490	1987.0	k_0 (Ar)	[47]
		2.048×10^{35}	−5.771	2130.1	k_0 (N_2)	[22], pw
		2.327×10^{34}	−5.520	1975.9	k_0 (O_2)	[22], pw
		6.488×10^{35}	−5.675	2572.1	k_0 (NH_3)	[22], pw
		9.629×10^{35}	−5.731	2651.9	k_0 (H_2O)	[22], pw
	Troe parameters: $\alpha = 0.31$, $T^{***} = 10^{-30}$, $T^{*} = 10^{30}$, $T^{**} = 10^{30}$					pw
R6	$H + O_2 (+M) \leftrightarrow HO_2 (+M)$	4.660×10^{12}	0.440	0.0	k_∞	[48]
		1.910×10^{20}	−1.557	253.9	k_0 (N_2)	[30]
		3.770×10^{18}	−0.713	−794.5	k_0 (NH_3)	[22], pw
	Troe parameters: $\alpha = 0.5$, $T^{***} = 1$, $T^{*} = 10^{10}$, $T^{**} = 10^{30}$					[30]
R7	$NH_2 + NO \leftrightarrow N_2 + H_2O$	2.600×10^{19}	−2.369	870.0		[49]
R8	$NH_2 + NO \leftrightarrow NNH + OH$	4.300×10^{10}	0.294	−866.0		[49]
R9	$NH_2 + NO_2 \leftrightarrow N_2O + H_2O$	2.601×10^{18}	−2.191	455.0		[50]
R10	$NH_2 + NO_2 \leftrightarrow H_2NO + NO$	9.095×10^{11}	0.032	−1512.1		[50]
R11	$NH + NO \leftrightarrow N_2O + H$	2.700×10^{15}	−0.780	20.0		[16]
R12	$NH + NO \leftrightarrow N_2 + OH$	6.800×10^{14}	−0.780	20.0		[16]
R13	$NH_2 + O \leftrightarrow HNO + H$	2.780×10^{13}	−0.065	−188.0		[51]
R14	$NH_2 + O \leftrightarrow NH + OH$	3.090×10^{3}	2.840	−2780.0		[51]
R15	$NH_2 + HO_2 \leftrightarrow OH + H_2NO$	1.566×10^{13}	0.000	0.0		[16]
R16	$NH_3 + O_2 \leftrightarrow NH_2 + HO_2$	1.415×10^{10}	1.285	55224.0		[41]
R17	$NH_3 + H \leftrightarrow NH_2 + H_2$	1.963×10^{4}	2.854	8520.2		[41]
R18	$NH_3 + OH \leftrightarrow NH_2 + H_2O$	1.559×10^{5}	2.372	118.9		[41]
R19	$NH_3 + O \leftrightarrow NH_2 + OH$	4.430×10^{2}	3.180	6739.9		[41]
R20	$NH_3 + HO_2 \leftrightarrow NH_2 + H_2O_2$	1.173×10^{0}	3.839	17260.0		[41]
R21	$NH_2 + O \leftrightarrow NO + H_2$	2.380×10^{12}	0.112	−347.0		[51]
R22	$NH + OH \leftrightarrow HNO + H$	1.510×10^{14}	−0.314	−308.0		[51]
R23	$NH + OH \leftrightarrow NO + H_2$	3.430×10^{13}	−0.303	−336.0		[51]
R24	$NH + OH \leftrightarrow N + H_2O$	2.610×10^{7}	1.660	−945.0		[51]
R25	$NH_2 + NH \leftrightarrow N_2H_2 + H$	4.260×10^{14}	−0.270	−77.5		[47]
R26	$HNO + H \leftrightarrow NO + H_2$	1.660×10^{10}	1.180	−446.0		[51]
R27	$tHNNO + H \leftrightarrow NH_2 + NO$	1.800×10^{13}	0.183	−45.0		[52]
R28	$tHNNO + H \leftrightarrow N_2 + H + OH$	1.200×10^{14}	−0.077	126.0		[52]
R29	$tHNNO + H \leftrightarrow N_2 + H_2O$	7.900×10^{13}	−0.139	270.0		[52]
R30	$tHNNO + H \leftrightarrow N_2O + H_2$	6.700×10^{6}	1.878	143.0		[52]
R31	$cHNNO + H \leftrightarrow NH_2 + NO$	5.800×10^{10}	0.313	−182.0		[52]
R32	$cHNNO + H \leftrightarrow N_2 + H + OH$	1.000×10^{14}	−0.157	180.0		[52]
R33	$cHNNO + H \leftrightarrow N_2 + H_2O$	9.100×10^{13}	−0.088	75.0		[52]

(*continued on next page*)

Table 2 (*continued*).

ID	Reaction	A	β	E_{act}	Notes	Ref.
R34	$cHNNO + H \leftrightarrow N_2O + H_2$	3.000×10^{13}	0.0954	60.0		[52]
R35	$N_2O + H (+M) \leftrightarrow tHNNO (+M)$	1.700×10^{4}	3.05	6530.0	k_∞	[53]
		1.300×10^{27}	−3.48	7030.0	k_0	
	Troe parameters: $\alpha = 0.12$, $T^{***} = 10^{-30}$, $T^{*} = 10^{30}$					
	Efficiencies: $H_2 = 3.0$, $H_2O = 21$, $O_2 = 1.1$, $N_2 = 1.5$					
R36	$N_2O + H (+M) \leftrightarrow cHNNO (+M)$	2.400×10^{-2}	4.81	4790.0	k_∞	[53]
		1.200×10^{25}	−2.94	6770.0	k_0	
	Troe parameters: $\alpha = 0.12$, $T^{***} = 10^{-30}$, $T^{*} = 10^{30}$					
	Efficiencies: $H_2 = 3.0$, $H_2O = 21$, $O_2 = 1.1$, $N_2 = 1.5$					
R37	$tHNNO (+M) \leftrightarrow cHNNO (+M)$	1.3×10^{4}	3.36	23000.0	k_∞	[53]
		1.0×10^{17}	−0.801	16900.0	k_0	
	Troe parameters: $\alpha = 0.074$, $T^{***} = 10^{-30}$, $T^{*} = 10^{30}$					
	Efficiencies: $H_2 = 3.0$, $H_2O = 21$, $O_2 = 1.1$, $N_2 = 1.5$					
R38	$N_2O + O \leftrightarrow NO + NO$	2.000×10^{10}	1.000	24800.0		[54,55]
R39	$N_2O + O \leftrightarrow N_2 + O_2$	2.600×10^{12}	0.500	41100.0		[54,55]
R40	$NH_3 + NO_2 \leftrightarrow HONO + NH_2$	2.211×10^{11}	0.0	24906.0		[56]
R41	$H_2NO + OH \leftrightarrow HNO + H_2O$	2.140×10^{15}	−0.751	−464.0		[57]
R42	$H_2NO + O_2 \leftrightarrow HNO + HO_2$	1.723×10^{5}	2.188	18010.0		[58]
R43	$H_2NO + NO_2 \leftrightarrow HONO + HNO$	7.946×10^{0}	2.950	−3292.6		[58]
R44	$H_2NO + NH_2 \leftrightarrow HNO + NH_3$	9.481×10^{12}	−0.081	−1643.4		[58]
R45	$H_2NO + HO_2 \leftrightarrow HNO + H_2O_2$	5.405×10^{4}	2.160	−3597.7		[58]
R46	$HNO + O_2 \leftrightarrow NO + HO_2$	2.000×10^{13}	0.000	15896.0		[46]
R47	$HNO + NO_2 \leftrightarrow HONO + NO$	7.900×10^{2}	3.060	3882.0		[59]

PLOG predictions and the fitted falloff expressions:

$$\mathrm{RMSLE} = \sqrt{\frac{1}{N}\sum_{i=1}^{N}\left[\ln(k_{\mathrm{falloff}}(T_i, P_i)) - \ln(k_{\mathrm{PLOG}}(T_i, P_i))\right]^2} \quad (1)$$

where N represents the total number of (T,P) evaluation points. Parameter bounds were enforced to ensure physical meaningfulness (e.g., $0 < \alpha \leq 1$ for TROE parameters, T^{***}, T^{*}, and $T^{**} > 0$, and positive pre-exponential factors). The optimization framework is able to include parameter fixing or specify bounds through a flexible configuration system, so to incorporate literature-derived constraints when available.

Through this approach, the resulting falloff expressions can reproduce the original PLOG behavior across the specified conditions, while keeping the mathematical structure required for efficient implementation in CHEMKIN-compatible solvers and subsequent mixture rule applications.

The collider efficiencies for the key reactions previously identified were obtained through an extensive literature analysis, including both comprehensive reviews [16,46] and recent experimental and theoretical studies. When specific collider data were not available, default efficiencies were assigned based on similar reactions. Moreover, to incorporate the recent findings by Glarborg and coworkers [21–23] on the temperature dependence of collision efficiencies for specific reactions, a spline-based functional representation $\alpha_{ij}(T)$ (efficiency of the jth species acting as collider in the ith reaction) was derived from the available discrete efficiency data points, most of the times provided at 300, 1000 and 2000 K. Using these functions, low-pressure limit rate constants were calculated as:

$$k^0_{ij}(T) = k^0_{i\text{-}ref}(T) \cdot \alpha_{ij}(T) \quad (2)$$

over 200 evenly spaced temperature points within the temperature range. The resulting $k^0_{ij}(T)$ values were refitted into a modified-Arrhenius form, i.e. the final expressions adopted in the kinetic mechanism, and shown in Table 2.

Where collider-specific pressure-dependent rates were not available, the parameters describing the falloff behavior were assumed as identical for each collider compared to the reference one. Although this is a simplification compared to the full LMR-R methodology, it is the most practical option currently supported within the CHEMKIN framework. The macroscopic impact of this approximation is quantified and critically assessed in Section 3.

2.3. Kinetic modeling

The kinetic model describing ammonia pyrolysis and oxidation, integrating the parametrized kinetic rates described above, was developed starting from the previous studies by Stagni et al. [33,41]. These earlier models were assembled following the hierarchy and modularity principles within the CRECK kinetic framework [62]. However, given the recent significant advancements in ammonia [6] and hydrogen [63] chemistry, substantial updates were incorporated into the NH_3 kinetic framework, including the latest theoretical calculations for relevant submechanisms. Additionally, thermodynamic properties for the NH_3 subset were updated based on the most recent ATcT recommendations [64]. Transport properties were retained from the previous works [33,41].

The core H_2-O_2 kinetics was upgraded to the latest Galway hydrogen mechanism [30,65,66]. This includes the reaction channel $HO_2 + HO_2 \rightarrow OH + OH + O_2$, recently investigated *ab initio* by Klippenstein et al. [63], and the subset describing the OH* chemiluminescence pathway [67–69].

The key reactions involved in the NH_2O potential energy surface, impacting both flame propagation (e.g. $NH_2 + O \rightarrow HNO + H$) and low-temperature kinetics (due to H_2NO formation) were revised based on the high-level theoretical predictions by Klippenstein et al. [51]. Furthermore, the NH_2 + HNO reaction, yielding NH_3 and NO, which was shown to play a role in inhibiting NH_3 oxidation, was updated after the recent study by Jian et al. [23].

Nitrogen selectivity pathways leading to NO and N_2O during ammonia oxidation were substantially revised following recent findings by Glarborg et al. [52] on the N_2O + H path via HNNO and the subsequent NH+NO channels. Specifically, the predictive capability for N_2O selectivity at high pressures was improved by explicitly introducing the two HNNO isomers (*cis* and *trans*) and incorporating their reactivity based on isomerization and decomposition rates from Meng et al. [53], combined with the HNNO + H reaction rates from Glarborg et al. [52]. The NH+NO reaction rate and branching ratio were selected from the comprehensive review work by Baulch et al. [16], reconciling a vast amount of available experimental data, still remaining consistent within uncertainty bounds estimated by Klippenstein et al. [70].

Finally, the low-temperature oxidation chemistry, still an open research field [6], was updated with regard to H_2NO-related reactions.

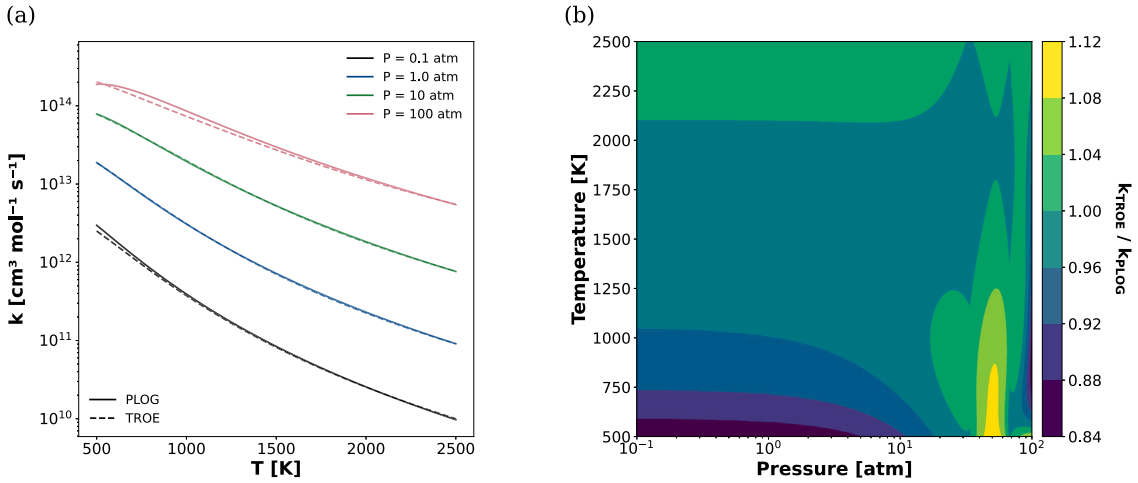

Fig. 1. (a) Comparison between the original rate R1 (k_{PLOG}) [41] and the parametrized rate (k_{TROE}). (b) Contour plot of the ratio between the two rates. N_2 is the reference collider.

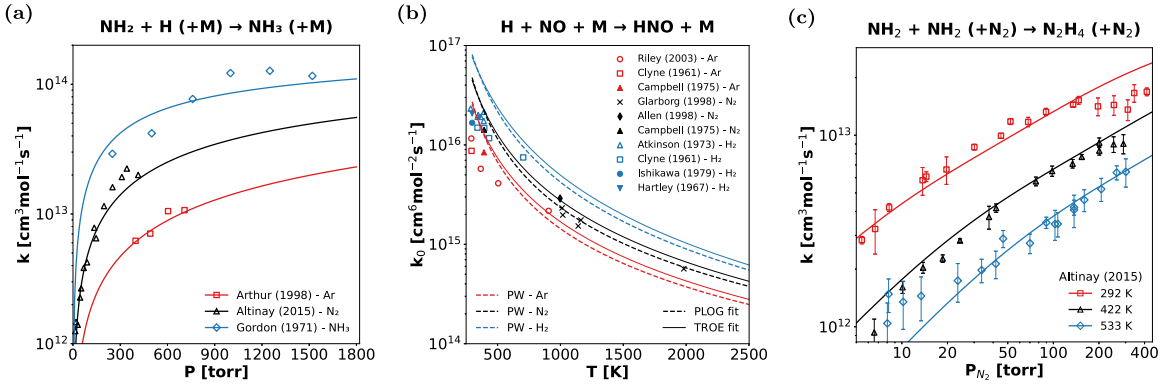

Fig. 2. Comparison between experimental data (symbols) [71–80] and modeling predictions (lines) for (a) R1 (at room temperature - cfr. [21]), (b) R2 (low-pressure limit) and (c) R5 with the different colliders.

Specifically, H-abstractions by O_2, HO_2, NO_2 and NH_2 were revised according to recent theoretical work by Stagni and Cavallotti [58], while the H-abstraction by OH was updated based on the latest calculations by Klippenstein and Glarborg [57]. Additional refinements, not discussed here for brevity, are summarized in Table 2. Although tuning the individual reaction rates within their estimated uncertainties is a possible follow-up of this activity to further improve the agreement with experimental data, such optimization was beyond the scope of this study and thus not performed.

The kinetic mechanism is available in CHEMKIN format in the Supplementary Material, as well as its comprehensive validation. Additionally, a version of the mechanism including the investigated rates with reduced-pressure linear mixture rules (Section 2.2) is provided in Cantera (`yaml`) format, which, to the authors' knowledge is the only standard currently fully supporting this feature.

3. Results and discussion

3.1. Rate constants

The rate constants for reactions R1–R4 listed in Table 2, identified through literature review and sensitivity analysis, were parametrized into TROE format following the procedure described in Section 2.2. Specifically, reactions R1 and R2 were parametrized after fitting the reverse rates, based on the corresponding rate constants computed at the *ab initio* level in the reference work [41], in PLOG format at the different pressure levels. To ensure physical consistency, the high-pressure limits for reactions R1, R2, and R3 were constrained to the respective rates previously calculated in previous studies [40,42,43]. On the other hand, for R4 no high-pressure rate was found in the literature; therefore, no constraint was imposed, and the high-pressure-limit Arrhenius parameters were considered as free optimization variables. Moreover, in the original work [46], R4 was estimated only at three pressure levels, namely 0.1, 1 and 10 atm; therefore, due to their limited number, this was the only case in which parametrization was performed in the Lindemann form instead of Troe, after summing the two dissociation pathways available in [46].

The rate parametrizations achieved satisfactory results for all of the 4 reactions. Fig. 1 shows representative results for the ammonia recombination reaction R1. The fitted rate differed from the original one by a factor ranging between 0.84 and 1.11. However, as shown in Fig. 1b, the deviation was much smaller through most of the operating space, with the ratio being consistently close to unity. The average deviation between the fitted and original rates was ~2.2%, much lower than the uncertainty factor of such rates (usually at least a factor of two [41,58]). Details regarding the parametrization of R2–R4 is provided in the Supplementary Material; their results are comparable to what obtained for R1.

Subsequently, the low-pressure limit rate constants for reactions R1, R2, R5 and R6 were refitted via Eq. (2). According to the sources, the reference collider was N_2 for all reactions except R5, for which Ar was selected. For reaction R6, due to the hierarchical formulation of the mechanism, only the low-pressure limit rate (k_0) for NH_3 was obtained,

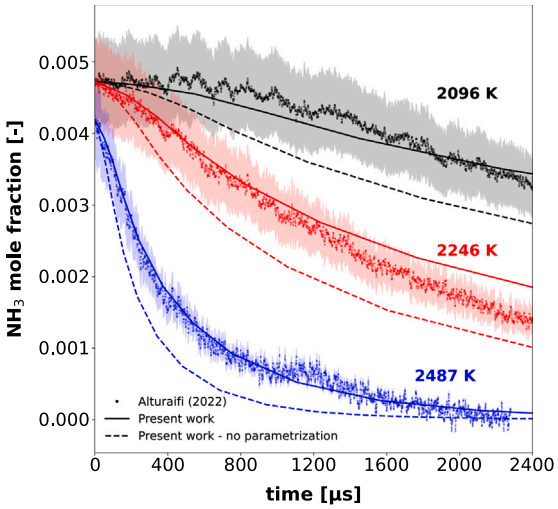

Fig. 3. NH_3 speciation profiles for a mixture of ~0.5% NH_3 in Ar (P = 1.2 atm) [81], and related prediction with and without reactions parametrization, i.e. with and without species-specific low-pressure limits for reactions from R1 to R6.

as the collision efficiency and/or the falloff behavior for the remaining colliders were already defined in the core mechanism [30].

Fig. 2 compares the collider-dependent rates predicted for reactions R1, R2 and R5 against the available experimental data. No experimental data were found instead for R6 with NH_3 as a collider. A reasonably good agreement is observed in all the comparisons, capturing both pressure dependence and collider-specific behaviors effectively. For HNO recombination (Fig. 2b), some deviations are evident at the lowest temperatures for H_2 and Ar. In particular, for H_2, the measured rates at ambient temperature seem to contradict the higher efficiency predicted theoretically (a factor ~1.7 at 300 K [23]). For Ar, the rate overestimates the experimental data at ambient temperature, too. Anyway, a significantly better agreement is observed at combustion-relevant temperatures for all three colliders. For the sake of completeness, Fig. 2b shows both the TROE-fitted k_0 and the corresponding low-pressure limit extrapolated from the original PLOG data. The maximum deviation is below 10% at the highest temperatures, while being almost overlapped for $T < 700$ K.

3.2. Colliders impact on pyrolysis and oxidation chemistry

Using a hierarchical approach, the impact of reaction parametrizations and collider-specific behaviors was first evaluated in pyrolysis conditions. Fig. 3 shows the mechanism validation against available speciation data for NH_3 pyrolysis, obtained in shock tube experiments [81]. It is possible to observe that the predicted NH_3 temporal profiles are particularly sensitive to collider-specific effects, with differences exceeding the 12% experimental uncertainty, especially emphasized at higher temperatures. The flux analysis under representative conditions (Fig. 4a) identified the key elementary steps leading from NH_3 to N_2. It is shown that pressure-dependent reactions play crucial roles, specifically ammonia decomposition (R1b) and the subsequent diazene (N_2H_2) decomposition into NNH and H (R4). Sensitivity analysis (Fig. 4b) points out that decomposition is primarily driven by NH_3 decomposition in the Ar bath gas, followed by N_2H_2 formation via R25 and its subsequent decomposition R4. Consequently, explicitly accounting for the weaker collider efficiency of Ar in R1 significantly slowed down the overall consumption rate of ammonia.

The intermediates of the pyrolysis process are also significantly affected by collider-specific parametrization: Fig. 5a and 5b show the

(a)

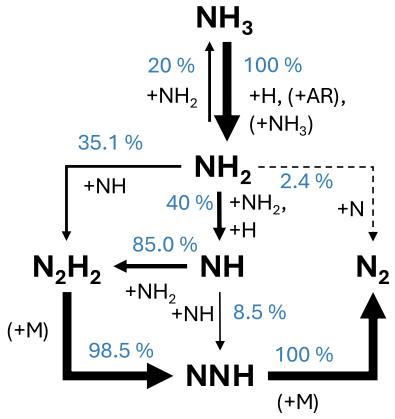

(b)

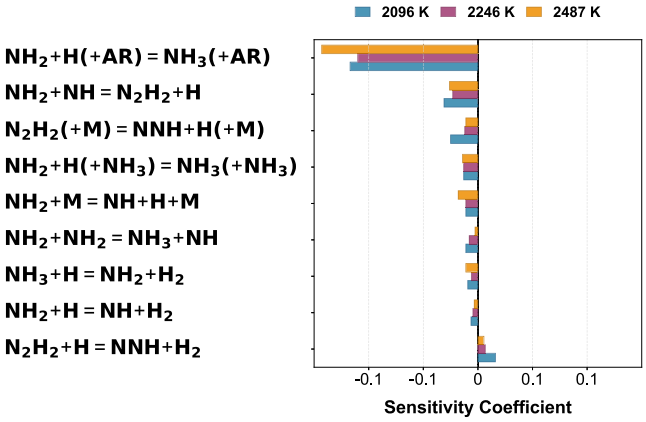

Fig. 4. NH_3 pyrolysis in a shock tube (cfr. Fig. 3). (a) Nitrogen flux analysis (T = 2096 K. t = 1200 μs), relative to the single molecule. (b) Sensitivity analysis to NH_3 mass fraction at times corresponding to ~10% conversion.

time profiles of NH_2 and NH, respectively, as measured by Davidson et al. [82]. This dataset has long served as a benchmark for the validation of ammonia pyrolysis mechanisms [6,30,83]. Clearly, incorporating collider effects in key reaction rates significantly affects the mechanism predictions, and neglecting such effects may mislead the tuning of other reaction rates due to error compensation. In this case, after incorporating the parametrized reactions without additional tuning, the NH_2 time evolution is predicted reasonably well, in terms of both peak time and overall trend. Conversely, especially the peak concentration of NH is somewhat underpredicted.

Moving to oxidation conditions, Fig. 6 shows the inhibiting effect of ammonia addition on the oxidation of lean H_2-O_2 mixtures, as observed experimentally and predicted numerically in a Jet-Stirred-Reactor configuration. The experimental trends are well captured by the kinetic model, showing a clear inhibition pattern due to ammonia addition in both Ar and N_2 bath gases. A slight delay in reactivity onset (~35 K without ammonia) is observed when using N_2 as the bath gas compared to Ar, which is correctly predicted, too. Such a configuration is an optimal benchmark for kinetic models as it can lead to oscillatory behaviors, due to the coupling between chemical kinetics, heat transfer, and mass transport, resulting in limit cycles consisting in repeated ignition and extinction [84–86]. In this case, a narrow oscillatory region was experimentally observed only for pure H_2, with both Ar and N_2 as bath gases. Such behavior is accurately predicted by the kinetic model, in terms of temperature window as well and average temperature rise, as well as H_2 and O_2 mole fractions.

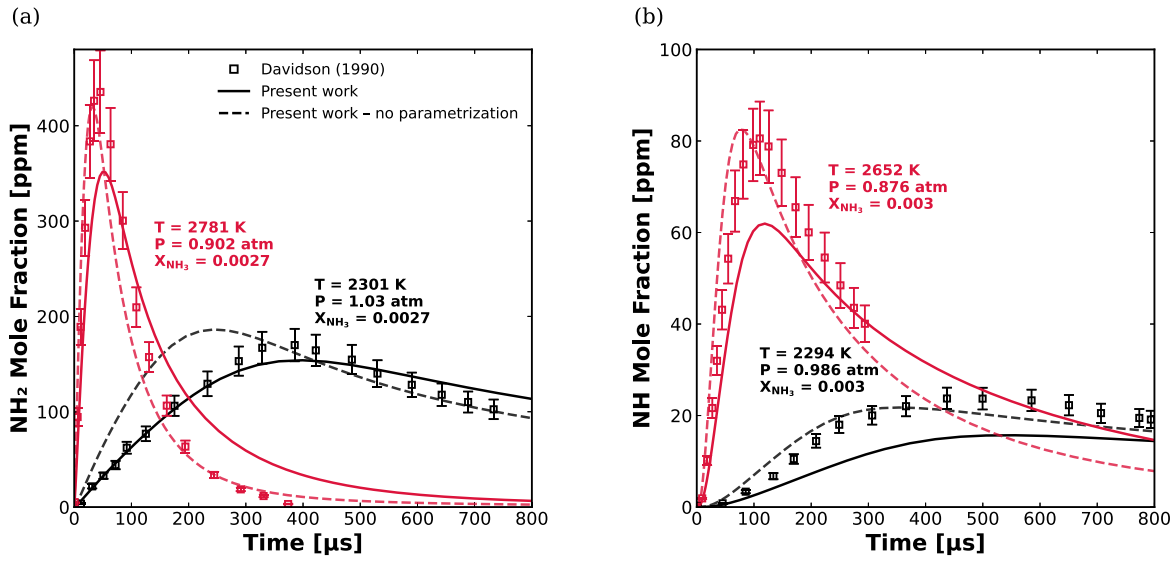

Fig. 5. (a) NH_2 and (b) NH species profiles in a mixture of NH_3 in Ar [82], and related predictions with and without reactions parametrization.

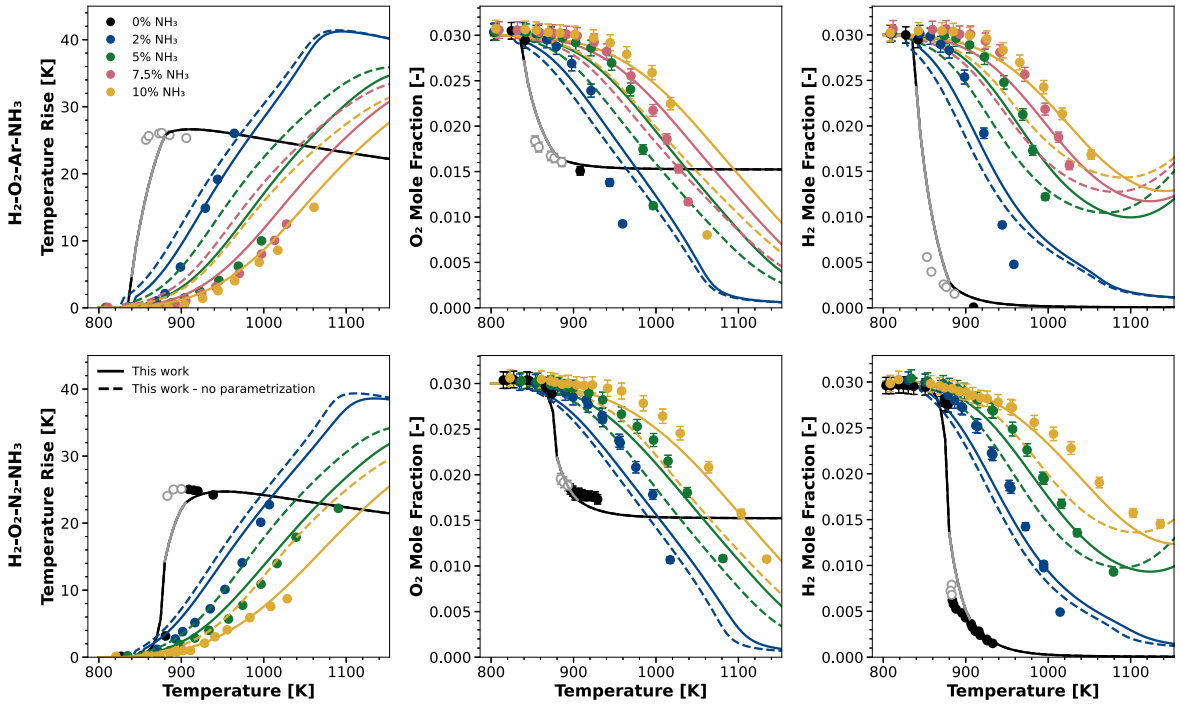

Fig. 6. Oxidation of H_2-O_2 mixtures at $\Phi = 0.5$, diluted in 94% Ar-NH_3 (top row) and 94% N_2-NH_3 bath gas, with different NH_3 concentration. Experimental data [19] vs numerical predictions. Gray symbols and lines indicate oscillating conditions, as identified experimentally and predicted by the model, respectively.

More importantly, the parametrization of pressure-dependent rates proved essential for accurately predicting the conversion rate and temperature rise as increasing amounts of NH_3 were added. Although the base model qualitatively predicts inhibition, it progressively loses accuracy when ammonia replaces the bath gas, and this discrepancy becomes increasingly pronounced with higher ammonia mole fractions. To shed light on this, Fig. 7 shows flux analysis with 0% and 10% NH_3 in N_2 environment, at the temperature corresponding to the same H_2 conversion (10%). Without ammonia (Fig. 7a), hydrogen follows its well-known oxidation pathway, undergoing H-abstraction by H and OH radicals, providing H atoms. These then react with O_2, either branching via $H + O_2 = O + OH$ or recombining through the pressure-dependent reaction R6.

When ammonia is added, it affects the hydrogen oxidation pathway to a significant extent, as shown in Fig. 7b. In these conditions, H_2 oxidation is promoted by the reverse H-abstraction from H_2 (R17). Subsequently, NH_3 undergoes its consolidated low-temperature oxidation path [41], starting from NH_2 radicals. NH_2 is converted into NO through the H_2NO path by reacting with NO_2 (R10) and HO_2 (R15), respectively, followed by HNO oxidation (R46). On the other hand, nitrogen selectivity towards N_2 is driven by the thermal DeNOx reaction R7, which acts as a radical termination, too.

Fig. 8 explains in detail the overall inhibiting effect of ammonia on hydrogen reactivity. Considering N_2 as reference bath gas, most inhibition is due to the previously discussed thermal DeNOx reaction R7 and from the reaction involving H-abstraction from NH_3 by O_2 R16, which

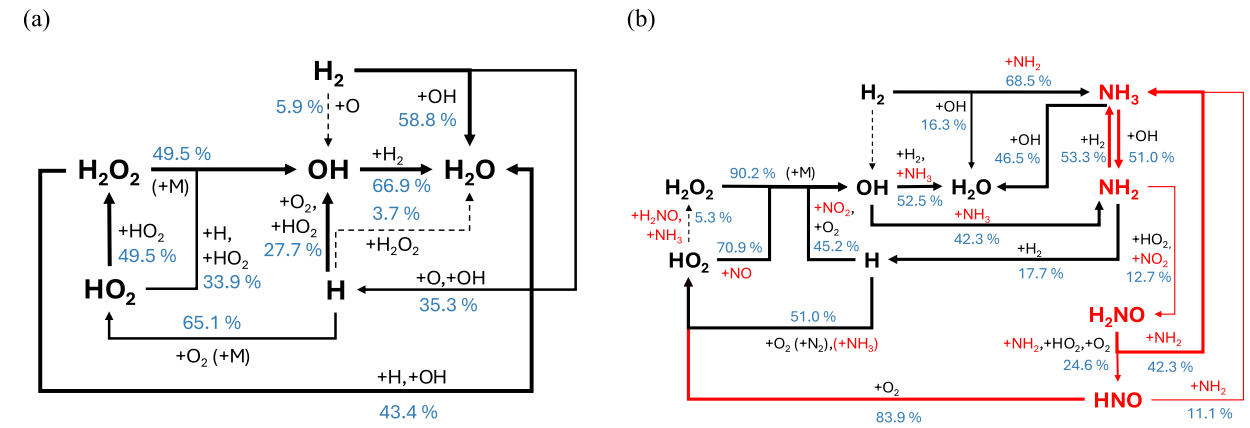

Fig. 7. Hydrogen flux analysis with (a) 0% and (b) 10% NH_3, performed at equal 10% H_2 conversion, with N_2 as bath gas (cfr. Fig. 6). Flux intensity is relative to the single molecule.

is reversed at low temperature and lean conditions (see also [41]). Above all, the recombination reaction H + O_2(+M) → HO_2(+M) (R6) is the third most important contribution to the observed inhibition. Although NH_3 concentration is one order of magnitude lower than N_2, the sensitivity of the recombination reaction with NH_3 as collider is comparable to the same reaction with N_2, the dominant bath gas. Therefore, while the base model qualitatively captures the chemical inhibition of ammonia, its partial quantitative accuracy can be related to the incomplete description of third-body effects. The parametrization of pressure-dependent reactions was able to explain the remaining effect, confirming the conclusions by Sabia et al. [19] about the major role of ammonia as a collider.

The effect of rate constant parametrization and resulting inclusion of third-body dependencies lead to nonlinear changes in the laminar flame propagation features, too, as shown in Fig. 9. Here, the models' output is compared against experimental data from Figueroa-Labastida et al. for pure NH_3 [87] and NH_3-H_2 blends [88] in an argon atmosphere. In most cases, the magnitude of the change in predictions resulting from parametrization is comparable to, or slightly exceeds, the experimental uncertainties. The largest deviations are observed in rich conditions, at higher hydrogen concentrations. It is interesting to note that such deviations exhibit a non-monotonic behavior, such that the updated model predicts lower flame speeds at high hydrogen contents, and vice versa when hydrogen content is reduced or absent.

Fig. 10 sheds light on such behavior: HNO dissociation (reverse R2) is one of the main drivers of flame propagation, as it provides H radicals, enhancing radical branching through the flame front. Including the effect of H_2O as a "strong collider" increases, as a net effect, the backward reaction rate. As R2 is particularly important in the flame propagation of pure ammonia (cfr. [41]), the updated model predicts slower flame speeds in these conditions. Conversely, as hydrogen fraction increases, the relative importance of this reaction decreases, causing the model to predict faster flames at higher H_2 contents. This deviation is more pronounced for rich mixtures, where the importance of ammonia recombination (R1, not shown in Fig. 10 due to lower sensitivity) progressively increases.

The nonlinear impact of third-body collider effects on laminar flame speed becomes apparent when varying the equivalence ratio, as shown in Fig. 11a for NH_3-air flames. Explicitly accounting for pressure- and collider-dependent reactions leads to higher predicted flame speeds in lean conditions, while at richer equivalence ratios the predicted speed becomes lower. Moreover, the inclusion of collider effects slightly shifts the peak flame speed towards stoichiometric conditions. Overall, although the observed deviations are still within the experimental uncertainty range, the inclusion of collider effects changes the shape of the flame speed curve. The sensitivity analysis in Fig. 11b provides further insight into this inversion: it can be seen that ammonia recombination

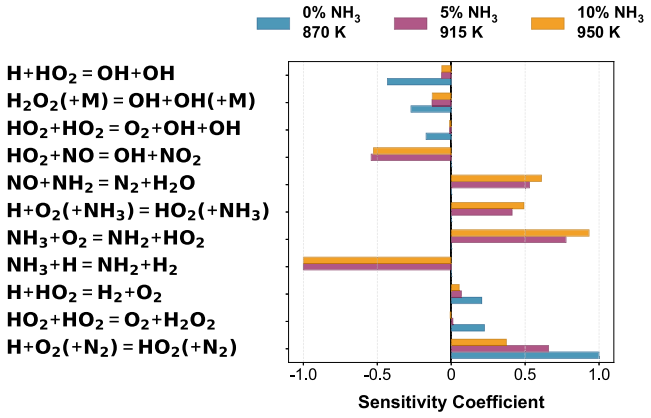

Fig. 8. Sensitivity coefficients to H_2 mass fractions, normalized with respect to the local maximum value, performed at equal 10% H_2 conversion with N_2 as bath gas (cfr. Fig. 6). For readability, the reaction H + O_2 = O + OH is omitted.

R1 and HNO decomposition (reverse R2) play key roles at rich and lean conditions, respectively, yet with opposite effects on flame propagation: while R1 reduces reactivity by depleting H and NH_2 radicals on the flame front, R2 enhances branching by feeding H radicals. Compared to the base model, both reactions exhibit increased rates, due to the role of H_2O as an efficient collider, whose concentration increases downstream of the flame front. Therefore, the flame propagation characteristics are shown to be significantly affected by the role of H_2O in the key pressure-dependent reactions, while other colliders, including NH_3, play a comparatively minor role. For completeness, the separate effect of each of the 4 reactions is shown in the Supplementary Material.

3.3. Impact of mixture rules

In this section, the macroscopic impact of adopting a simplified treatment on mixture rules on the overall predictive capability of the ammonia mechanism is considered in detail. Reactions R1, R2, R5, and R6, previously identified as critical also by Singal et al. [29] in their recent work, were modeled via LMR-R. It is important to note that for the first three reactions, temperature- and pressure-dependent rates $k_i(T, P)$ were available only for a single reference collider, thus temperature-dependent collision efficiencies were added

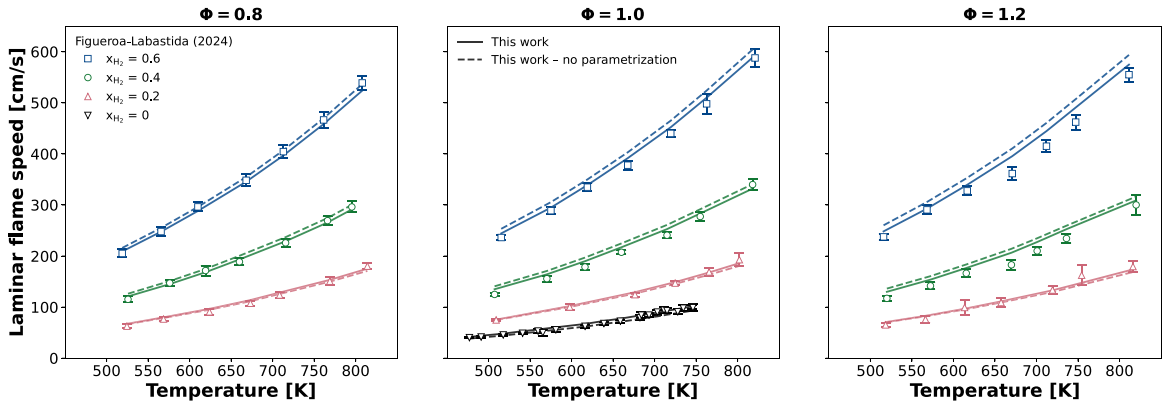

Fig. 9. Laminar flame speed of NH_3 and NH_3-H_2 mixtures at variable T_u and Φ, in an Ar-O_2 atmosphere (79:21 mol/mol). Experimental data from Figueroa-Labastida et al. [87,88].

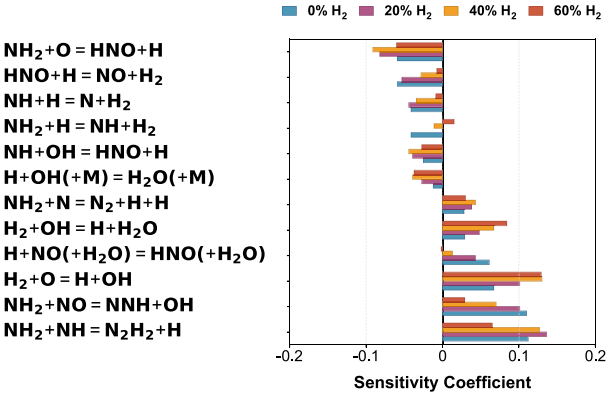

Fig. 10. Sensitivity coefficients to laminar flame speed of NH_3 and NH_3-H_2 mixtures, at T_u = 650 K and P = 1 atm, in an Ar-O_2 atmosphere (79:21 mol/mol). For readability, the reaction $H + O_2 = O + OH$ is omitted.

for the species for which they had been calculated. For R6, temperature-dependent collision efficiency was added only for NH_3, as efficiencies and pressure-dependent rates are already available for other colliders (and $k_{Ar}(T,P)$, $k_{N_2}(T,P)$ and $k_{He}(T,P)$ are uniquely defined, too). Singal et al. also applied LMR-R treatment to H + OH (+M) ↔ H_2O (+M) and OH + OH (+M) ↔ H_2O_2 (+M), but they were not considered in this work as not belonging to the NH_3 mechanism, nor data on ammonia as a collider were available for these reactions.

As a theoretical comparison, Fig. 12 compares the rate constants of NH_3 decomposition (R1b) predicted with and without the LMR-R formulation, at 1, 10 and 100 atm. Randomly sampled initial temperatures and molar compositions (with mixtures of NH_3, O_2, N_2, H_2O and Ar) were chosen. Consistent with the formulation in Table 1, both approaches provide very similar results at low pressures. Deviations occur in the fall-off region and become more pronounced closer the high-pressure limit, especially at the lowest temperatures where this limit is reached earlier. Nevertheless, up to combustion-relevant conditions (around 100 atm), the average deviation of R1b remains within 30%. However, although qualitatively the same behavior is expected for all the pressure-dependent reactions, on a quantitative basis the agreement between the two models depends on the high-pressure limit and fall-off behavior of each specific reaction.

Fig. 13 compares the predicted laminar flame speeds for NH_3 and NH_3-H_2 flames in air at variable pressures and equivalence ratios. Using the LMR-R mixture rules generally yields slightly higher flame speeds: at ambient conditions, predictions are nearly identical between the two formulations. As expected, the largest relative deviations are observed at elevated pressure and increased H_2 fractions, and keep increasing with pressure (a further comparison is available in the SM). However, in the 1-10 bar range, the differences between the two modeling approaches are always comparable to (or lower than) the experimental uncertainty of the reference data. Moreover, unlike the effect observed when introducing collider parametrization (Fig. 11a), changing the mixture rule does not significantly affect the overall shape of the flame speed curves.

To get further insight on this behavior, Fig. 14 compares the mole fraction profiles of three key radicals, i.e. H, NH_2 and HNO, mostly involved in the pressure-dependent reactions, along the flame axial coordinate. The same figure also shows the related overall reaction rates (R1, R2 and R6, respectively), which significantly affect flame propagation (cfr. Fig. 11b), as predicted by the two mixture models. The peak reaction rates differ by at most 10% at 10 bar. The higher flame speed predicted via LMR-R approach can be primarily attributed to the lower overall reaction rate of R1 (cfr. Fig. 12), in spite of the higher concentrations of both NH_2 and H radicals. This is thus a direct consequence of employing LMR-R as mixing rule.

This analysis was completed by analyzing constant-volume ignition delay times of NH_3-O_2 mixtures in the widest possible range of operating conditions. A parametric study was performed by varying (i) temperature, (ii) pressure, (iii) equivalence ratio, (iv) dilution ratio and (v) type of diluent. Fig. 15 summarizes the most important findings for two pure bath gases (N_2 and H_2O) and two intermediate N_2/H_2O mixtures, in rich conditions. In this analysis, the ignition delay time was defined as the time corresponding to the maximum pressure rise. It can be observed that the deviations between the two methodologies do not exceed 10%, typically remaining below 5% through most of the parametric space, and are found at lower mole fractions of more efficient colliders (H_2O in this case). The strong similarity in the predictions between the two approaches must be attributed to the relative sensitivity of the 4 reactions across the operating conditions. As shown in several previous studies [30,33,41], out of the 4 investigated reactions, ignition delay time is sensitive only to R1 and R2, and especially at higher temperatures. Conversely, at higher temperatures the difference between the rates with and without LMR-R treatment is the smallest one, as shown in Fig. 12. However, such comparisons might change once a wider set of key reactions for ignition (e.g. R4) becomes available. To date, the bottleneck in this process is indeed the availability of collider-specific efficiencies outside of the reactions subset investigated here (and those previously mentioned related to the core H_2 chemistry).

Additional case studies, including a sensitivity analysis to each of the 4 rates modeled here, as well as laminar flame propagation and speciation comparisons, are presented in the Supplementary Material.

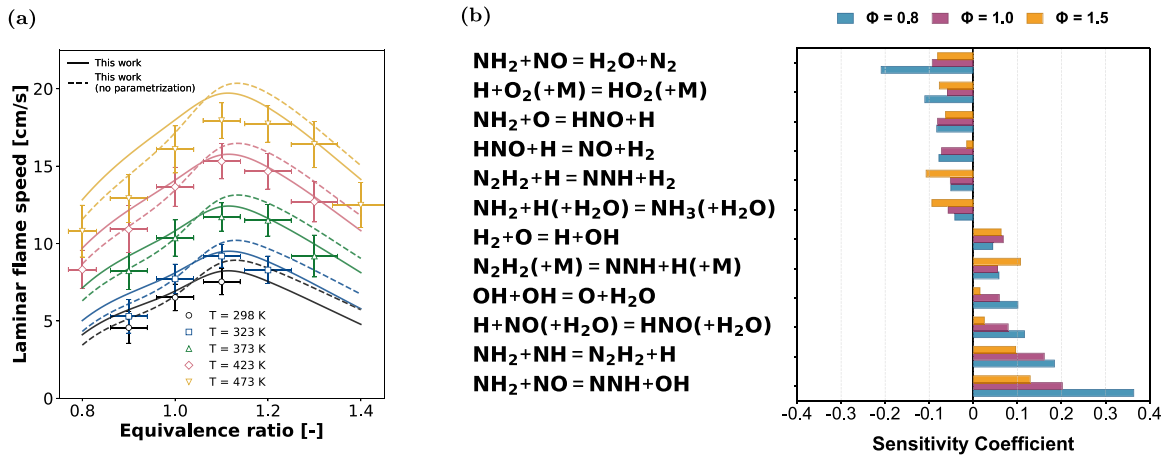

Fig. 11. (a) Laminar flame speeds of NH_3-air mixtures at atmospheric pressure: experimental data [89] vs modeling results, performed with and without rate parametrization. (b) Sensitivity analysis at T_u = 373 K and variable Φ.

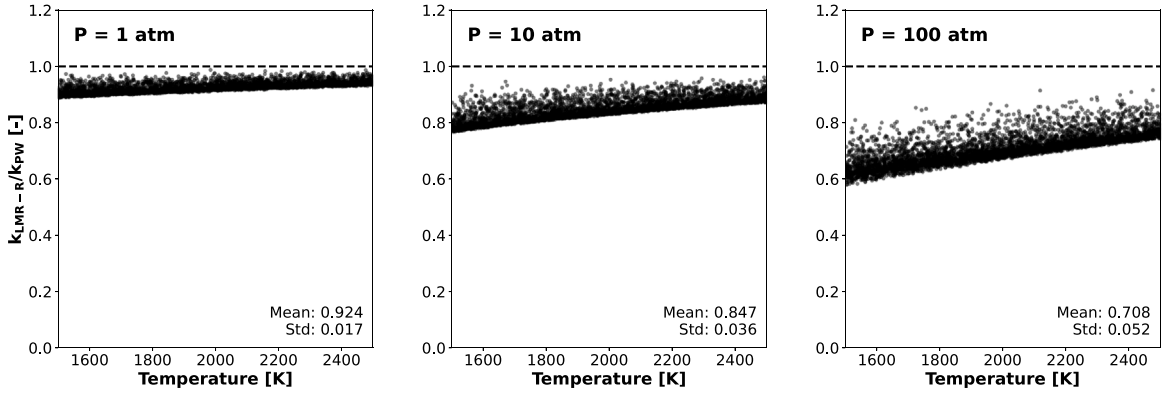

Fig. 12. Ratio k_{LMR-R}/k_{PW} for R1b at fixed pressures and variable temperature, considering 15,000 random compositions (5000 per pressure) of NH_3, O_2, N_2, Ar and H_2O, as evaluated via independent colliders ("This work") and LMR-R mixture rule ("LMR-R").

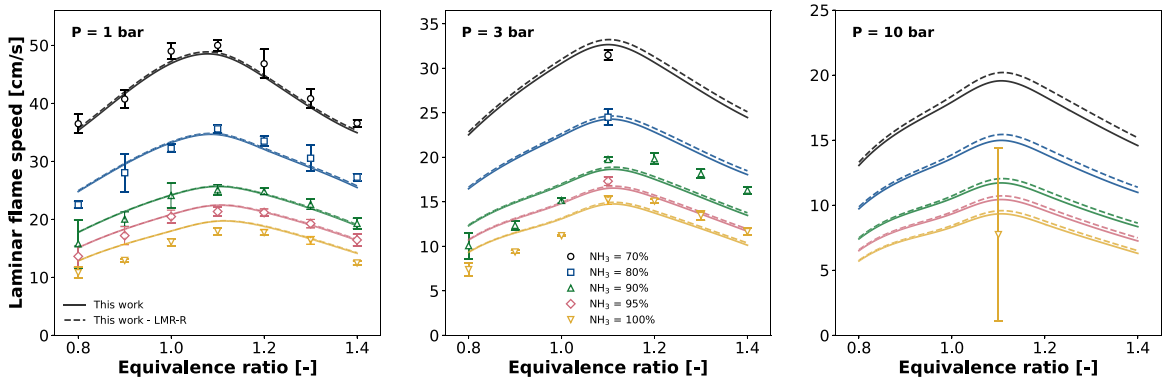

Fig. 13. Laminar flame speeds of NH_3-H_2-air mixtures at variable pressure (T_u = 473 K): experimental data [90] vs modeling results, with and without the inclusion of reduced-pressure mixture rules.

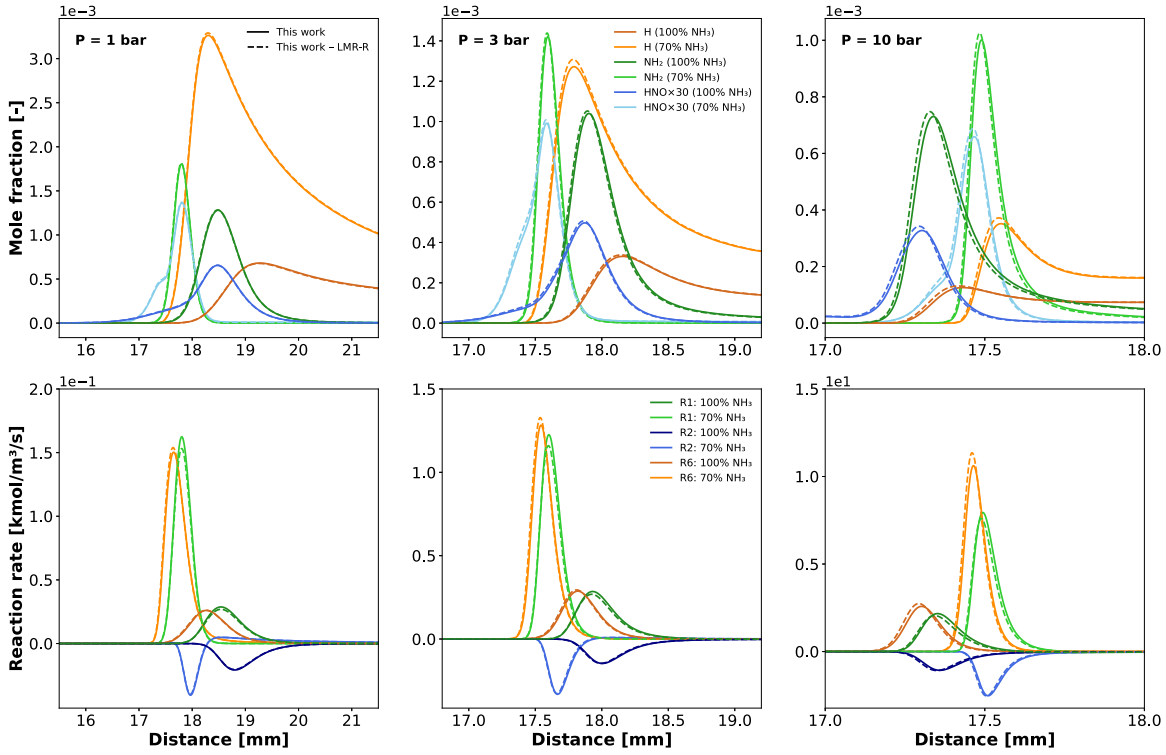

Fig. 14. Laminar flame speeds of NH_3-H_2-air mixtures (Φ = 1.1 - cfr. Fig. 13), at variable pressure and NH_3-H_2 blending ratio. Top row: mole fraction of the major species involved in pressure-dependent reactions, with and without the inclusion of reduced-pressure mixture rules. Bottom row: major pressure-dependent reaction rates, evaluated with and without the inclusion of reduced-pressure mixture rules.

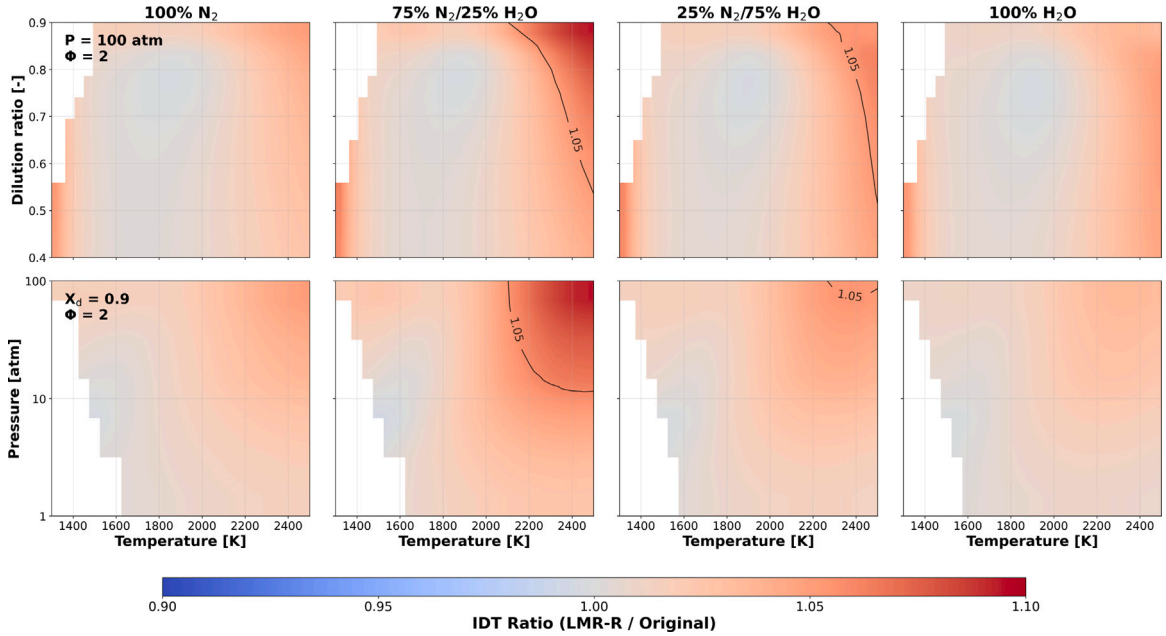

Fig. 15. Ratio between predicted ignition delay times, with and without the inclusion of reduced-pressure mixture rules. Top row: variable temperature and dilution ratio. Bottom row: variable temperature and pressure. The region where ignition delay time exceeded 5 ms (white background) was excluded from the analysis.

4. Conclusions

In spite of remarkable progress achieved in the kinetic modeling of ammonia pyrolysis and oxidation over the past decade, significant challenges must still be overcome to ensure accurate predictions across the broadest range of operating conditions. In this context, pressure-dependent reactions have received significant experimental and theoretical attention. However, their specific roles in ammonia combustion chemistry, as well as the individual contributions of the single colliders, had not been systematically investigated until now.

In this work, these gaps were addressed by setting up a comprehensive, integrated workflow. Pressure-dependent reactions mostly affecting ammonia chemistry were first identified in different conditions, including ignition, speciation and flame propagation. At a second stage, the role of third-body colliders was incorporated by combining recent high-level theoretical calculations, performed for reference bath gases, with temperature-dependent collision efficiencies, recently obtained via trajectory-based approaches. Although TROE parametrization might, in principle, be not always suitable for pressure-dependent reactions involving complex potential energy surfaces, it proved effective for fitting the key rates involved in ammonia kinetics, with negligible average errors (~2%–3%), especially when compared to the intrinsic uncertainties associated with the underlying theoretical calculations. These rates were integrated into a detailed kinetic framework, properly updated according to the most recent literature findings.

The extensive benchmarking of the kinetic mechanism provided important insights into the impact of such rates, as well as the specific roles of the different colliders. The most significant effect was observed with regard to speciation, in both pyrolysis and oxidation conditions. In pyrolysis conditions, the largest impact resulted from the ammonia decomposition reaction: this was primarily due to the lower efficiency of argon, which is commonly used as bath gas in fundamental experiments, but its reduced efficiency as a collider has received limited attention in kinetic modeling studies. Moreover, the inhibiting role of NH_3 in stirred conditions, experimentally observed when NH_3 was co-fueled with hydrogen, found theoretical support in the role of ammonia itself as a collider in the $H + O_2$ recombination, which subtracts H radicals from the branching reaction $H+O_2 = O+OH$. This provided theoretical support to the previous hypotheses regarding its strong collider behavior in these conditions.

When considering flame propagation, the macroscopic effect of introducing collider parametrization was generally comparable to the experimental uncertainty. However, this effect significantly changed with the equivalence ratio and, in the case of NH_3-H_2 flames, with the blending ratio. Specifically, the opposite effects of NH_3 recombination and HNO decomposition, both parametrized in this work, resulted in opposite variations at lean and rich conditions, causing a slight shift of the peak flame speed towards stoichiometric conditions. In both scenarios, H_2O emerged as the major key collider responsible for this change.

Finally, multiple bath-gas effects were investigated by assessing the impact of reduced-pressure mixture rules against the conventional linear mixing. While at higher pressures important deviations were found in the single rates (e.g. NH_3 dissociation), the effect on the predicted flame propagation was generally within the range of experimental uncertainties. The peak reaction rates along the flame coordinate showed changes of at most 10% when employing the most accurate model. Also, when predicting ignition delay times, deviations were still within 10%, which were more significant when strong colliders (H_2O) were involved in lower amounts within a less-efficient bath gas. This was primarily attributed to the sensitivity of the four rates who underwent LMR-R treatment (especially NH_3 and HNO dissociation), peaking at the highest temperatures, where the difference between the two rates is anyway smaller. Such results may anyway change once collider-specific efficiencies become available for a larger set of reactions, which is currently the bottleneck preventing a wider utilization of the LMR-R methodology.

However, it is important to emphasize that, due to the hierarchical approach in kinetic mechanism development [62], the parametrization was performed only for the reactions directly related to NH_3 chemistry. In this case, and to the authors' knowledge, no specific fall-off behavior is currently available in literature. Thus, the same reduced-pressure dependence as the reference collider was assumed, but with a different efficiency [29]. Further experimental or theoretical studies providing detailed collider-specific fall-off behavior would be highly beneficial, as could potentially change the observed deviations between the two modeling approaches.

CRediT authorship contribution statement

Alessandro Stagni: Writing – original draft, Methodology, Formal analysis, Conceptualization. **Timoteo Dinelli:** Writing – review & editing, Software, Methodology, Investigation, Formal analysis, Conceptualization.

Declaration of competing interest

The authors declare that they have no known competing financial interests or personal relationships that could have appeared to influence the work reported in this paper.

Acknowledgments

This work was supported by the EU Horizon Europe Research and Innovation Programme under the HORIZON-MSCA-2023-DN-01 GA No 101169263. Views and opinions expressed are however those of the authors only and do not necessarily reflect those of the European Union or European Research Executive Agency (REA). Neither the European Union nor the granting authority can be held responsible for them.

Appendix A. Supplementary data

Supplementary material related to this article can be found online at https://doi.org/10.1016/j.cej.2025.170737.

Data availability

Data (kinetic mechanism) and details about the codes are provided in the Supplementary Material.

References

[1] A. Valera-Medina, H. Xiao, M. Owen-Jones, W.I. David, P.J. Bowen, Ammonia for power, Prog. Energy Combust. Sci. 69 (2018) 63–102.
[2] H. Kobayashi, A. Hayakawa, K.K.A. Somarathne, E.C. Okafor, Science and technology of ammonia combustion, Proc. Combust. Inst. 37 (1) (2019) 109–133.
[3] W.S. Chai, Y. Bao, P. Jin, G. Tang, L. Zhou, A review on ammonia, ammonia-hydrogen and ammonia-methane fuels, Renew. Sustain. Energy Rev. 147 (2021) 111254.
[4] J.A. Miller, C.T. Bowman, Mechanism and modeling of nitrogen chemistry in combustion, Prog. Energy Combust. Sci. 15 (4) (1989) 287–338.
[5] P. Glarborg, J.A. Miller, B. Ruscic, S.J. Klippenstein, Modeling nitrogen chemistry in combustion, Prog. Energy Combust. Sci. 67 (2018) 31–68.
[6] M. Monge-Palacios, X. Zhang, N. Morlanes, H. Nakamura, G. Pezzella, S.M. Sarathy, Ammonia pyrolysis and oxidation chemistry, Prog. Energy Combust. Sci. 105 (2024) 101177.
[7] A. Alnasif, S. Mashruk, H. Shi, M. Alnajideen, P. Wang, D. Pugh, A. Valera-Medina, Evolution of ammonia reaction mechanisms and modeling parameters: A review, Appl. Energy Combust. Sci. 15 (2023) 100175.
[8] A.G. Szanthoffer, I.G. Zsély, L. Kawka, M. Papp, T. Turányi, Testing of NH_3/H_2 and NH_3/syngas combustion mechanisms using a large amount of experimental data, Appl. Energy Combust. Sci. 14 (2023) 100127.

[9] S. Girhe, A. Snackers, T. Lehmann, R. Langer, F. Loffredo, R. Glaznev, J. Beeckmann, H. Pitsch, Ammonia and ammonia/hydrogen combustion: Comprehensive quantitative assessment of kinetic models and examination of critical parameters, Combust. Flame 267 (2024) 113560.

[10] H.J. Curran, Developing detailed chemical kinetic mechanisms for fuel combustion, Proc. Combust. Inst. 37 (1) (2019) 57–81.

[11] M.C. Barbet, M.P. Burke, Impact of missing third-body efficiencies on kinetic model predictions of combustion properties, Proc. Combust. Inst. 38 (1) (2021) 425–432.

[12] A. Stagni, F.R. Artioli, A. Frassoldati, The role of radiative heat loss and collisional energy transfer in the flammability limits of NH_3 and NH_3–H_2 mixtures, Ind. Eng. Chem. Res. 63 (50) (2024) 21805–21815.

[13] J. Zádor, S.J. Klippenstein, J.A. Miller, Pressure-dependent OH yields in alkene + HO_2 reactions: a theoretical study, J. Phys. Chem. A 115 (36) (2011) 10218–10225.

[14] J.A. Miller, S.J. Klippenstein, Master equation methods in gas phase chemical kinetics, J. Phys. Chem. A 110 (36) (2006) 10528–10544.

[15] C. Cavallotti, M. Pelucchi, Y. Georgievskii, S.J. Klippenstein, Estoktp: electronic structure to temperature-and pressure-dependent rate constants—a code for automatically predicting the thermal kinetics of reactions, J. Chem. Theory Comput. 15 (2) (2018) 1122–1145.

[16] D. Baulch, C.T. Bowman, C.J. Cobos, R.A. Cox, T. Just, J. Kerr, M. Pilling, D. Stocker, J. Troe, W. Tsang, et al., Evaluated kinetic data for combustion modeling: supplement ii, J. Phys. Chem. Ref. Data 34 (3) (2005) 757–1397.

[17] F. Battin-Leclerc, J.M. Simmie, E. Blurock, Cleaner combustion, developing detailed chemical kinetic models, in: Series: Green Energy and Technology, Springer International Publishing AG, Cham, 2013.

[18] A. Bertolino, A. Frassoldati, A. Cuoci, A. Parente, Estimation of third body efficiencies from experimental data: Application to hydrogen combustion, Int. J. Hydrog. Energy 48 (63) (2023) 24504–24520, http://dx.doi.org/10.1016/j.ijhydene.2023.03.173.

[19] P. Sabia, M.V. Manna, R. Ragucci, M. de Joannon, Mutual inhibition effect of hydrogen and ammonia in oxidation processes and the role of ammonia as strong collider in third-molecular reactions, Int. J. Hydrog. Energy 45 (56) (2020) 32113–32127.

[20] M.V. Manna, P. Sabia, G. Sorrentino, T. Viola, R. Ragucci, M. de Joannon, New insight into nh3-h2 mutual inhibiting effects and dynamic regimes at low-intermediate temperatures, Combust. Flame 243 (2022) 111957.

[21] P. Glarborg, H. Hashemi, S. Cheskis, A.W. Jasper, On the rate constant for $NH_2 + HO_2$ and third-body collision efficiencies for $NH_2 + H(+M)$ and $NH_2 + NH_2(+M)$, J. Phys. Chem. A 125 (7) (2021) 1505–1516.

[22] A.W. Jasper, Predicting third-body collision efficiencies for water and other polyatomic baths, Faraday Discuss. 238 (2022) 68–86.

[23] J. Jian, H. Hashemi, H. Wu, P. Glarborg, A.W. Jasper, S.J. Klippenstein, An experimental, theoretical, and kinetic modeling study of post-flame oxidation of ammonia, Combust. Flame 261 (2024) 113325.

[24] S.J. Klippenstein, From theoretical reaction dynamics to chemical modeling of combustion, Proc. Combust. Inst. 36 (1) (2017) 77–111.

[25] L. Lei, M.P. Burke, Bath gas mixture effects on multichannel reactions: Insights and representations for systems beyond single-channel reactions, J. Phys. Chem. A 123 (3) (2018) 631–649.

[26] L. Lei, M.P. Burke, Mixture rules and falloff are now major uncertainties in experimentally derived rate parameters for $H + O_2(+M) = HO_2(+M)$, Combust. Flame 213 (2020) 467–474.

[27] L. Lei, M.P. Burke, Dynamically evaluating mixture effects on multi-channel reactions in flames: A case study for the $CH_3 + OH$ reaction, Proc. Combust. Inst. 38 (1) (2021) 433–440.

[28] M.P. Burke, R. Song, Evaluating mixture rules for multi-component pressure dependence: $H + O_2(+M) = HO_2(+M)$, Proc. Combust. Inst. 36 (1) (2017) 245–253.

[29] P.J. Singal, J. Lee, L. Lei, R.L. Speth, M.P. Burke, Implementation of new mixture rules has a substantial impact on combustion predictions for H_2 and NH_3, Proc. Combust. Inst. 40 (1–4) (2024) 105779.

[30] Y. Zhu, H.J. Curran, S. Girhe, Y. Murakami, H. Pitsch, K. Senecal, L. Yang, C.-W. Zhou, The combustion chemistry of ammonia and ammonia/hydrogen mixtures: A comprehensive chemical kinetic modeling study, Combust. Flame 260 (2024) 113239.

[31] E. Ramalli, G. Scalia, B. Pernici, A. Stagni, A. Cuoci, T. Faravelli, Data ecosystems for scientific experiments: managing combustion experiments and simulation analyses in chemical engineering, Front. Big Data 4 (2021) 663410.

[32] E. Ramalli, T. Dinelli, A. Nobili, A. Stagni, B. Pernici, T. Faravelli, Automatic validation and analysis of predictive models by means of big data and data science, Chem. Eng. J. 454 (2023) 140149.

[33] A. Stagni, S. Arunthanayothin, M. Dehue, O. Herbinet, F. Battin-Leclerc, P. Bréquigny, C. Mounaïm-Rousselle, T. Faravelli, Low-and intermediate-temperature ammonia/hydrogen oxidation in a flow reactor: Experiments and a wide-range kinetic modeling, Chem. Eng. J. 471 (2023) 144577.

[34] R. Gilbert, K. Luther, J. Troe, Theory of thermal unimolecular reactions in the fall-off range. ii. weak collision rate constants, Berichte Bunsenges. Phys. Chem. 87 (2) (1983) 169–177.

[35] P. Stewart, C. Larson, D. Golden, Pressure and temperature dependence of reactions proceeding via a bound complex. 2. application to 2ch3→ c2h5+ h, Combust. Flame 75 (1) (1989) 25–31.

[36] J. Troe, V.G. Ushakov, Revisiting falloff curves of thermal unimolecular reactions, J. Chem. Phys. 135 (5) (2011).

[37] P.K. Venkatesh, A.Y. Chang, A.M. Dean, M.H. Cohen, R.W. Carr, Parameterization of pressure-and temperature-dependent kinetics in multiple well reactions, AIChE J. 43 (5) (1997) 1331–1340.

[38] L. Lei, M.P. Burke, Evaluating mixture rules and combustion implications for multi-component pressure dependence of allyl+ ho2 reactions, Proc. Combust. Inst. 37 (1) (2019) 355–362.

[39] D.G. Goodwin, H.K. Moffat, I. Schoegl, R.L. Speth, B.W. Weber, Cantera: An object-oriented software toolkit for chemical kinetics, thermodynamics, and transport processes, 2024, http://dx.doi.org/10.5281/zenodo.14455267, https://www.cantera.org, version 3.1.0.

[40] P. Glarborg, H. Hashemi, P. Marshall, Challenges in kinetic modeling of ammonia pyrolysis, Fuel Commun. 10 (2022) 100049.

[41] A. Stagni, C. Cavallotti, S. Arunthanayothin, Y. Song, O. Herbinet, F. Battin-Leclerc, T. Faravelli, An experimental, theoretical and kinetic-modeling study of the gas-phase oxidation of ammonia, React. Chem. Eng. 5 (4) (2020) 696–711.

[42] W. Tsang, J.T. Herron, Chemical kinetic data base for propellant combustion i. reactions involving NO, NO_2, HNO, HNO_2, HCN and N_2O, J. Phys. Chem. Ref. Data 20 (4) (1991) 609–663.

[43] D. Fulle, H. Hamann, H. Hippler, J. Troe, Temperature and pressure dependence of the addition reactions of ho to no and to NO_2. iv. saturated laser-induced fluorescence measurements up to 1400 bar, J. Chem. Phys. 108 (13) (1998) 5391–5397.

[44] X. Chen, M.E. Fuller, C.F. Goldsmith, Decomposition kinetics for hono and hno 2, React. Chem. Eng. 4 (2) (2019) 323–333.

[45] P. Glarborg, The $NH_3/No_2/O_2$ system: Constraining key steps in ammonia ignition and N_2O formation, Combust. Flame 257 (2023) 112311.

[46] A.M. Dean, J.W. Bozzelli, Combustion chemistry of nitrogen, in: Gas-Phase Combustion Chemistry, Springer, 2000, pp. 125–341.

[47] S.J. Klippenstein, L. Harding, B. Ruscic, R. Sivaramakrishnan, N. Srinivasan, M.-C. Su, J. Michael, Thermal decomposition of NH_2OH and subsequent reactions: ab initio transition state theory and reflected shock tube experiments, J. Phys. Chem. A 113 (38) (2009) 10241–10259.

[48] R.X. Fernandes, K. Luther, J. Troe, V.G. Ushakov, Experimental and modelling study of the recombination reaction H O2 (M) –> HO_2 (M) between 300 and 900 k, 1.5 and 950 bar, and in the bath gases m=he, ar, and N_2, Phys. Chem. Chem. Phys. 10 (29) (2008) 4313–4321.

[49] S. Song, R. Hanson, C. Bowman, D. Golden, Shock tube determination of the overall rate of NH_2 + NO -> products in the thermal de-NOx temperature window, Int. J. Chem. Kinet. 33 (11) (2001) 715–721.

[50] S.J. Klippenstein, L.B. Harding, P. Glarborg, Y. Gao, H. Hu, P. Marshall, Rate constant and branching fraction for the $NH_2 + NO_2$ reaction, J. Phys. Chem. A 117 (37) (2013) 9011–9022.

[51] S.J. Klippenstein, C.R. Mulvihill, P. Glarborg, Theoretical kinetics predictions for reactions on the NH_2O potential energy surface, J. Phys. Chem. A 127 (41) (2023) 8650–8662.

[52] P. Glarborg, E. Fabricius-Bjerre, T.K. Joensen, H. Hashemi, S.J. Klippenstein, An experimental, theoretical and kinetic modeling study of the N_2O-H_2 system: Implications for N2O H, Combust. Flame 271 (2025) 113810.

[53] Q. Meng, L. Lei, J. Lee, M.P. Burke, On the role of HNNO in NOx formation, Proc. Combust. Inst. 39 (1) (2023) 551–560.

[54] M. González, R. Sayos, R. Valero, Ab initio and kinetics study of the ground 1a potential energy surface of the O(1D) N2O –> 2 NO, N2 O2 (a1δg) reactions, Chem. Phys. Lett. 355 (1–2) (2002) 123–132.

[55] P. Glarborg, J.S. Allingham, A.B. Skov, H. Hashemi, P. Marshall, Re-examination of the N2O + O reaction, J. Phys. Chem. A 127 (31) (2023) 6521–6531.

[56] A.G. Thaxton, C.-C. Hsu, M.-C. Lin, Rate constant for the $NH_3 + NO_2$ –> NH_2 + HONO reaction: Comparison of kinetically modeled and predicted results, Int. J. Chem. Kinet. 29 (4) (1997) 245–251.

[57] S.J. Klippenstein, P. Glarborg, Theoretical kinetics predictions for $NH_2 + HO_2$, Combust. Flame 236 (2022) 111787.

[58] A. Stagni, C. Cavallotti, H-abstractions by O_2, NO_2, NH_2, and HO_2 from H_2NO: Theoretical study and implications for ammonia low-temperature kinetics, Proc. Combust. Inst. 39 (1) (2023) 633–641.

[59] Y. Shang, J. Shi, H. Ning, R. Zhang, H. Wang, S. Luo, Ignition delay time measurements and kinetic modeling of CH_4 initiated by CH_3NO_2, Fuel 243 (2019) 288–297.

[60] J. Bradbury, R. Frostig, P. Hawkins, M.J. Johnson, C. Leary, D. Maclaurin, G. Necula, A. Paszke, J. VanderPlas, S. Wanderman-Milne, Q. Zhang, Jax: composable transformations of python+numpy programs, 2018, software available from github.com/google/jax, URL http://github.com/google/jax.

[61] J. Nocedal, S.J. Wright, Numerical Optimization, second ed. in: Springer series in operations research, Springer, New York, 2006.

[62] M. Mehl, M. Pelucchi, L.P. Maffei, A. Stagni, A. Cuoci, A. Frassoldati, E. Ranzi, T. Faravelli, Developing chemical kinetic models for thermochemical applications, Nat. Protoc. (2025) 1–54.

[63] S.J. Klippenstein, R. Sivaramakrishnan, U. Burke, K.P. Somers, H.J. Curran, L. Cai, H. Pitsch, M. Pelucchi, T. Faravelli, P. Glarborg, $H\dot{O}_2 + H\dot{O}_2$: High level theory and the role of singlet channels, Combust. Flame 243 (2022) 111975.
[64] B. Ruscic, R.E. Pinzon, G. Von Laszewski, D. Kodeboyina, A. Burcat, D. Leahy, D. Montoy, A.F. Wagner, Active thermochemical tables: thermochemistry for the 21st century, J. Phys.: Conf. Ser. 16 (2005) 561, IOP Publishing.
[65] S. Panigrahy, A.A.E.-S. Mohamed, P. Wang, G. Bourque, H.J. Curran, When hydrogen is slower than methane to ignite, Proc. Combust. Inst. 39 (1) (2023) 253–263.
[66] J. Liu, S. Zhou, P. Wang, Y. Murakami, A.A.E.-S. Mohamed, M. Raza, A. Nolte, K.A. Heufer, P.K. Senecal, H.J. Curran, An experimental and kinetic modeling study of the ignition of methane/n-decane blends, Combust. Flame 272 (2025) 113884.
[67] T. Kathrotia, M. Fikri, M. Bozkurt, M. Hartmann, U. Riedel, C. Schulz, Study of the H + O + M reaction forming OH*: Kinetics of OH* chemiluminescence in hydrogen combustion systems, Combust. Flame 157 (7) (2010) 1261–1273.
[68] C.R. Mulvihill, E.L. Petersen, Oh* chemiluminescence in the h2no2 and h2n2o systems, Combust. Flame 213 (2020) 291–301.
[69] W. Sun, Q. Zhao, H.J. Curran, F. Deng, N. Zhao, H. Zheng, S. Kang, X. Zhou, Y. Kang, Y. Deng, et al., Further insights into the core mechanism of H2/CO/NOx reaction system, Combust. Flame 245 (2022) 112308.
[70] S.J. Klippenstein, L.B. Harding, P. Glarborg, J.A. Miller, The role of NNH in NO formation and control, Combust. Flame 158 (4) (2011) 774–789.
[71] M. Clyne, B. Thrush, Reaction of hydrogen atoms with nitric oxide, Trans. Faraday Soc. 57 (1961) 1305–1314.
[72] D.B. Hartley, B.A. Thrush, The rates of elementary processes in the chain reaction between hydrogen and oxygen iii. kinetics of the combination of hydrogen atoms with nitric oxide, Proc. R. Soc. Lond. Ser. A. Math. Phys. Sci. 297 (1451) (1967) 520–533.
[73] R. Atkinson, R. Cvetanović, Determination of the rates of hydrogen atom reaction with no by a modulation technique, Can. J. Chem. 51 (3) (1973) 370–372.
[74] I.M. Campbell, B.J. Handy, Studies of reactions of atoms in a discharge flow stirred reactor. part 1.—the o+ h 2+ no system, J. Chem. Soc. Faraday Trans. 1: Phys. Chem. Condens. Phases 71 (1975) 2097–2106.
[75] Y.-i. Ishikawa, K.-i. Sugawara, S. Sato, The rate constants for h and d-atom additions to o2, no, acetylene, and 1 3-butadiene, Bull. Chem. Soc. Japan 52 (12) (1979) 3503–3506.
[76] N. Arthur, I. Cooper, M. Gershenzon, V. Lozovsky, Recombination of nh2 radicals with hydrogen atoms, Chem. Phys. Rep. 17 (6) (1998) 1075–1087.
[77] P. Glarborg, M. Østberg, M.U. Alzueta, K. Dam-Johansen, J.A. Miller, The recombination of hydrogen atoms with nitric oxide at high temperatures, in: Symposium (International) on Combustion, vol. 27, Elsevier, 1998, pp. 219–226.
[78] M.T. Allen, R.A. Yetter, F.L. Dryer, Hydrogen/nitrous oxide kinetics—implications of the nxhy species, Combust. Flame 112 (3) (1998) 302–311.
[79] P.S. Riley, B. Cosic, A. Fontijn, The h+ no recombination reaction over a wide temperature range, Int. J. Chem. Kinet. 35 (8) (2003) 374–380.
[80] G. Altinay, R.G. Macdonald, Determination of the rate constants for the nh2 (x2b1)+ nh2 (x2b1) and nh2 (x2b1)+ h recombination reactions in n2 as a function of temperature and pressure, J. Phys. Chem. A 119 (28) (2015) 7593–7610.
[81] S.A. Alturaifi, O. Mathieu, E.L. Petersen, An experimental and modeling study of ammonia pyrolysis, Combust. Flame 235 (2022) 111694.
[82] D.F. Davidson, K. Kohse-Höinghaus, A.Y. Chang, R.K. Hanson, A pyrolysis mechanism for ammonia, Int. J. Chem. Kinet. 22 (5) (1990) 513–535.
[83] X. Zhang, S.P. Moosakutty, R.P. Rajan, M. Younes, S.M. Sarathy, Combustion chemistry of ammonia/hydrogen mixtures: Jet-stirred reactor measurements and comprehensive kinetic modeling, Combust. Flame 234 (2021) 111653.
[84] M. De Joannon, P. Sabia, A. Tregrossi, A. Cavaliere, Dynamic behavior of methane oxidation in premixed flow reactor, Combust. Sci. Technol. 176 (5–6) (2004) 769–783.
[85] M. Lubrano Lavadera, Y. Song, P. Sabia, O. Herbinet, M. Pelucchi, A. Stagni, T. Faravelli, F. Battin-Leclerc, M. De Joannon, Oscillatory behavior in methane combustion: influence of the operating parameters, Energy Fuels 32 (10) (2018) 10088–10099.
[86] A. Stagni, Y. Song, L.A. Vandewalle, K.M. Van Geem, G.B. Marin, O. Herbinet, F. Battin-Leclerc, T. Faravelli, The role of chemistry in the oscillating combustion of hydrocarbons: An experimental and theoretical study, Chem. Eng. J. 385 (2020) 123401.
[87] M. Figueroa-Labastida, L. Zheng, J.W. Streicher, R.K. Hanson, Ammonia/hydrogen laminar flame speed measurements at elevated temperatures, Int. J. Hydrog. Energy 63 (2024) 1137–1146.
[88] M. Figueroa-Labastida, L. Zheng, A.M. Ferris, N. Obrecht, C. Callu, R.K. Hanson, Shock-tube laminar flame speed measurements of ammonia/airgon mixtures at temperatures up to 771k, Combust. Flame 260 (2024) 113256.
[89] C. Lhuillier, P. Brequigny, N. Lamoureux, F. Contino, C. Mounaïm-Rousselle, Experimental investigation on laminar burning velocities of ammonia/hydrogen/air mixtures at elevated temperatures, Fuel 263 (2020) 116653.
[90] K.P. Shrestha, C. Lhuillier, A.A. Barbosa, P. Brequigny, F. Contino, C. Mounaïm-Rousselle, L. Seidel, F. Mauss, An experimental and modeling study of ammonia with enriched oxygen content and ammonia/hydrogen laminar flame speed at elevated pressure and temperature, Proc. Combust. Inst. 38 (2) (2021) 2163–2174.